

REPORT DOCUMENTATION PAGE			Form Approved OMB No. 0704-0188	
Public reporting burden for this collection of information is estimated to average 1 hour per response, including the time for reviewing instructions, searching existing data sources, gathering and maintaining the data needed, and completing and reviewing the collection of information. Send comments regarding this burden estimate or any other aspect of this collection of information, including suggestions for reducing this burden, to Washington Headquarters Services, Directorate for Information Operations and Reports, 1215 Jefferson Davis Highway, Suite 1204 Arlington, VA 22202-4302 and to the Office of Management and Budget, Paperwork Reduction Project (0704-0188), Washington, DC 20503.				
1. AGENCY USE ONLY (Leave blank)		2. REPORT DATE Feb 97	3. REPORT TYPE AND DATES COVERED Final 1 Nov 93 - 31 May 96	
4. TITLE AND SUBTITLE Analysis of Analog Airgun/Sonobuoy Records: A New Appraisal of the Variation of Upper Crustal Seismic Velocity with Age			5. FUNDING NUMBERS G N00014-94-1-0144	
6. AUTHOR(S) Richard L. Carlson Brian P. Cerney				
7. PERFORMING ORGANIZATION NAME(S) AND ADDRESS(ES) Texas A&M Research Foundation Box 3578 College Station, TX 77843			8. PERFORMING ORGANIZATION REPORT NUMBER 8661	
9. SPONSORING/MONITORING AGENCY NAME(S) AND ADDRESS(ES) Office of Naval Research Ballston Tower One 800 North Quincy Street Arlington, VA 22217-5660			10. SPONSORING/MONITORING AGENCY REPORT NUMBER	
11. SUPPLEMENTARY NOTES				
12a. DISTRIBUTION/AVAILABILITY STATEMENT <div style="border: 1px solid black; padding: 5px; width: fit-content; margin: 10px auto;"> DISTRIBUTION STATEMENT A  Approved for public release;  Distribution Unlimited </div>			12b. DISTRIBUTION CODE	
13. ABSTRACT (Maximum 200 words)  Analog sonobuoy records shot over 0 - 10 m.y. old crust along the East Pacific Rise have been digitally scanned, scaled, and analyzed for upper crustal velocity structure. Previous analyses of the original analog records [e.g., <i>Houtz and Ewing</i> , 1976] suggested that the average velocity of layer 2A at the EPR is 3.4 km/s and increases with age to about 4.5 km/s in 40-m.y.-old crust. Later work [ <i>Diebold and Carlson</i> , 1993] suggests that arrivals interpreted by <i>Houtz and Ewing</i> [1976] as representing layer 2A headwaves are actually diffractions and/or converted shear-waves. By digitally processing and analyzing many of the original analog records shot near the EPR, we have shown that (1) true layer 2A headwave arrivals are not present in these records, (2) the layer 2A retrograde branch reported in ESPs and other surveys cannot be resolved, and (3) layer 2B/3 velocities and average velocity gradients directly determined from the data range from 4.4 to 7.6 km/s and 1.1 to 2.2 /s, respectively. Because direct estimates of 'layer 2A' velocities are not possible, the linear gradient approximation for the hidden layer [ <i>Ewing and Purdy</i> , 1982] was applied; estimated velocities at the top of the basement section range from 2.0 to 3.1 km/s and velocity gradients are in the range 1.9 to 3.4 /s. These results show considerable scatter, and no relationship between velocities in the uppermost part of the oceanic crust and age of the crust can be resolved.				
14. SUBJECT TERMS			15. NUMBER OF PAGES 28	
			16. PRICE CODE	
17. SECURITY CLASSIFICATION OF REPORT UNCLASSIFIED	18. SECURITY CLASSIFICATION OF THIS PAGE UNCLASSIFIED	19. SECURITY CLASSIFICATION OF ABSTRACT UNCLASSIFIED	20. LIMITATION OF ABSTRACT UL	

**Analysis of Airgun/Sonobuoy Records:  
A New Appraisal of the Variation of Upper Crustal  
Seismic Velocity with Age**

**N00014-94-1-0144  
TAMRF 8661**

**FINAL REPORT**

**by**

**Richard L. Carlson**

**and**

**Brian P. Cerney**

**Department of Geology & Geophysics  
Texas A&M University  
College Station, TX 77843-3115**

**19970321 091**

**DTIC QUALITY INSPECTED 8**

Analog sonobuoy records shot over 0 - 10 m.y. old crust along the East Pacific Rise have been digitally scanned, scaled, and analyzed for upper crustal velocity structure. Previous analyses of the original analog records [e.g., *Houtz and Ewing*, 1976] suggested that the average velocity of layer 2A at the EPR is 3.4 km/s and increases with age to about 4.5 km/s in 40-m.y.-old crust. Later work [*Diebold and Carlson*, 1993] suggests that arrivals interpreted by *Houtz and Ewing* [1976] as representing layer 2A headwaves are actually diffractions and/or converted shear-waves. By digitally processing and analyzing many of the original analog records shot near the EPR, we have shown that (1) true layer 2A headwave arrivals are not present in these records, (2) the layer 2A retrograde branch reported in ESPs and other surveys cannot be resolved, and (3) layer 2B/3 velocities and average velocity gradients directly determined from the data range from 4.4 to 7.6 km/s and 1.1 to 2.2 /s, respectively. Because direct estimates of 'layer 2A' velocities are not possible, the linear gradient approximation for the hidden layer [*Ewing and Purdy*, 1982] was applied; estimated velocities at the top of the basement section range from 2.0 to 3.1 km/s and velocity gradients are in the range 1.9 to 3.4 /s. These results show considerable scatter, and no relationship between velocities in the uppermost part of the oceanic crust and age of the crust can be resolved.

## Introduction

During the 1960s, ships of the Lamont Doherty Geological Observatory collected over 500,000 km of variable-offset airgun sonobuoy profiles from the world's oceans. This dataset is the most complete suite of data characterizing the *in-situ* velocity structure of the upper oceanic crust and sediment cover. The data-collection technique involved launching a passive expendable sonobuoy while the ship was underway. This sonobuoy would remain relatively stationary in the water. While moving at a speed of about 6 knots (11 km/hr), the ship would tow a 25 cu. in. airgun firing at 11 second intervals. The seismic signal would be received by the launched sonobuoy and transmitted back to the

ship via an FM transmitter-receiver system [*LePichon et al.*, 1968]. In addition, a second sonobuoy was towed 200 m behind the air gun and recorded a normal incidence profile. The recorded analog data was bandpass filtered (5-20 Hz) and plotted as sign-bit traces on thermally sensitive paper. Figure 1 shows an example of the final data output.

The upper oceanic crust consists of "layers" 2A and 2B/2C. "Layers" 2A and 2B/2C are generally accepted to be composed of pillow basalts and sheeted dikes, respectively. The concept of a layered crust originated from ophiolite studies and analyses of early refraction surveys [e.g., *Raitt*, 1963; *Talwani et al.*, 1971; *Houtz and Ewing*, 1976; *Houtz*, 1976; *Salisbury and Christensen*, 1978]. With the advances of seismic acquisition techniques (e.g., multi-channel seismic methods and ocean-bottom sources and/or receivers) and analyses of the resultant data, this layered crust concept has been replaced by a crust whose physical properties vary continuously with depth [*Vera et al.*, 1990; *Rohr et al.*, 1990; *Carlson and Herrick*, 1990; *Vera and Diebold*, 1994; *Johnson and Semyan*, 1994; *Kappus et al.*, 1995].

There have been many published interpretations of portions of this sonobuoy data [e.g., *LePichon et al.*, 1968; *Houtz et al.*, 1968, 1970; *Ewing and Purdy*, 1982; *Vera and Mutter*, 1988] but only two published interpretations of a large portion of the existing data [*Houtz et al.*, 1970; *Houtz and Ewing*, 1976]. *Houtz and Ewing* [1976] interpreted approximately 220 paper sections using the slope-intercept method and concluded that they observed definite upper crustal velocity variations as a function of plate age; namely, that seismic layer 2A velocities increase "from about 3.3 km/s at the ridge crests to that of layer 2B on crust about 40 m.y. old." Since their publication, *Houtz and Ewing's* [1976] results have been debated [e.g. *Jacobson*, 1992; *Diebold and Carlson*, 1993; *Carlson and Jacobson*, 1994]. The purpose of this research is to reinterpret a portion of the sonobuoy dataset and to reevaluate the results. The sonobuoy records used in this study are from seismic profiles shot over 0-10 M.y. old crust from the plates surrounding the East Pacific Rise (EPR) between 20°S and 20°N (see Figure 2).

## Data

From the sonobuoy record shown in Figure 1, it can be seen that the data is quite noisy. This noisiness can be attributed to the weak signal sourced by a small 25 cu. in. airgun and received at the sonobuoy. During the course of data recording, the gain setting was changed as an attempt to increase the recording of the weak received signals. This gain change has had the effect of increasing not only the signal, but also the noise. This gain change can be seen in Figure 1 at approximately 3.7 km offset.

The analog sonobuoy seismograms were recorded as sign-bit traces (i.e., without amplitude). The only information contained in the traces are positive and negative values recorded as black and white as a function of offset and twt. Therefore, waveform analyses could not be made on this dataset. Another obvious feature of the data are the reverberations seen from the received signals. The reverberations were deliberately engineered and produced at the source to enhance the appearance and interpretability of the recorded signals. This has been useful in picking the arrivals on the records.

In addition to the recording enhancements and type of signal recorded on the seismograms, various sets of signals can be seen in the data. These sets can be separated into three categories: 1) seafloor reflections, 2) direct wave arrivals, and 3) refracted wave arrivals. Each category has one trait in common; namely, that their twt increases as a function of offset. The seafloor reflections are seen as a hyperbola, concave downward (towards increasing twt) and emerging from the zero offset trace. The direct wave arrivals are first seen at zero offset and zero twt, and are linear with an inverse slope equal to the speed of sound in water. Any deviations in the ship's course while it steamed away from the sonobuoy can be seen as departures from linearity in the direct wave arrivals. The third category, the refracted arrivals, are a bit more subtle on the sonobuoy records. They are clearly visible only as branches emanating from the seafloor reflection and are concave upward (i.e., toward decreasing twt). These refracted arrivals are generally not tangent to

the seafloor reflection at their point of intersection. This implies that the first refracted wave signal that was received and is observed adjacent to the seafloor reflection has been turned at a depth significantly greater than the seafloor. Thus, waves turned at shallower depths would be seen as secondary arrivals behind, or later than, the refracted arrivals and/or the seafloor reflections [cf. *Stephen*, 1982]. These secondary arrivals from shallow turning waves are not readily visible in the sonobuoy records.

## Analysis

Initially, the sonobuoy records were digitally scanned and scaled at Lamont-Doherty Geological Observatory. These digital images were then interpreted within a commercially available software package. Interpretation of the images on the computer involved digitization of each of the three categories of the seismic data mentioned above (i.e., the seafloor reflections, the direct wave arrivals, and the refracted wave arrivals). These digitized points (offset-twt pairs) were then used to construct oceanic crustal velocity models based on the assumption of stacked, linear velocity gradient layers. These velocity gradients were allowed to vary as a function of depth. In addition, the model layers were assumed to parallel the seafloor and were assumed to be laterally homogeneous. These simplifying assumptions seem reasonable, considering the single source-receiver configuration of the data collection and the non-uniqueness of modeling more complicated models.

Initially, the human errors in picking the precise locations of the arrivals of the signals on the sonobuoy records were determined. This was performed by picking a single observed arrival ten times at the same offset and then repeating the procedure at three other offsets. A plot of the digitized picks and their associated standard deviations in precision, or repeatability, of picking is shown in Figure 3. The conclusion here is that the average standard deviation in the human picking precision is slightly less than 3.0 ms. With this in mind, a check on the linearity of the direct wave arrival can now be made. This linearity,

or lack thereof, will allow for appropriate static shifts to the data to be made if the observed deviations from linearity in the direct wave arrivals are greater than or equal to the error in human digital picking. At some offsets, the deviation in linearity observed for the direct wave arrivals is greater than the human digital picking error. This means, that based on the analysis of the direct wave arrivals, appropriate static shifts to the sonobuoy data can be made. Static shifts have been applied to individual traces to correct for deviations in the course of the ship and drift of the sonobuoy.

The seafloor reflection is the next dataset category to be analyzed from the sonobuoy records. The seafloor reflection curve was used to model the normal incidence water depth and the apparent average dip of the seafloor over each seismic survey. The average absolute dips of the seafloor range from  $0.0^{\circ}$  -  $5.1^{\circ}$  with a mean of  $1.5^{\circ} \pm 1.4^{\circ}$ . The average dip of the seafloor calculated from each sonobuoy record will be taken into account when modeling the velocity structure of the crustal layers.

The velocity structure of the crustal layers can be modeled from analyses of the refracted wave arrivals. This third category of data, the refracted arrivals, contains information about the velocity structure and possible layering of the upper oceanic crust. The basic question of concern here is: Assuming parallel layering and lateral homogeneity, what upper crustal velocity structure model could give rise to the observed refracted arrivals? As mentioned earlier, there is generally a lack of tangency between the reflected and refracted arrivals at their point of intersection. This implies that waves turned just below the seafloor are not being observed as first arrivals on many of the sonobuoy records. If this is the case, then arrivals from these shallow turned waves may be second or third arrivals and thus appear to be masked by the seafloor reflection and/or the primary refracted arrivals. Since the airgun source was deliberately engineered to provide air bubble oscillations and to give rise to the apparent ringing in the data, the second or higher-order arrivals are not clearly visible. As an attempt to separate the first arrivals from the higher-order arrivals, some of the sonobuoy records were transformed to the tau-p domain.

An example of a sonobuoy record transformed to the tau-p domain is shown in Figure 4 [cf. *Vera and Mutter*, 1988]. It is clear from this figure that not much information, if any, has been gained through this transformation of the data. The noisiness and ringing in the data appears to have sufficiently masked these higher-order arrivals. Thus, arrivals from waves turned at shallow depths are not observed on the sonobuoy records. To model the upper crustal velocity structure from this dataset, assumptions about the velocity structure of the shallow crust where arrivals are masked, must be made. Following the "hidden layer" method of *Ewing and Purdy* [1982], it is assumed that the uppermost velocity structure of the crust consists of a single layer with a linear velocity gradient that is a function of depth.

The hidden layer approximation is a simplistic assumption that involves modeling only four parameters, the thickness, the velocity at the top, the velocity at the bottom, and the linear velocity gradient within the hidden layer. The general velocity model and ray path diagram for the hidden layer model is shown in Figure 5. A straightforward calculation of these parameters is discussed in *Ewing and Purdy* [1982]. One of the parameters, the velocity at the base of the hidden layer, can be directly measured from the sonobuoy record. It is equal to the inverse slope of the refraction branch at the point of intersection of the reflected and refracted arrivals. The other three parameters can be found by solving the following set of equations:

$$T(X) = t_0 + \frac{1}{K_1} \ln \left[ \frac{2v_1 + K_1 x_1}{2v_1 - K_1 x_1} \right] \quad (1)$$

$$h_1 = \frac{v_1}{K_1} - \sqrt{\left( \frac{v_1}{K_1} \right)^2 - \left( \frac{x_1}{2} \right)^2} \quad (2)$$

$$t_0 = \frac{2h_w + x_0 \sin \theta}{v_w \sqrt{1 - p^2 v_w^2}} \quad (3)$$

and 
$$x_0 = \frac{2h_w p v_w}{\sqrt{1 - p^2 v_w^2} - \sin \theta} \quad (4)$$

(modified from *Nettleton* [1940]) where  $p$ , the ray parameter, equals the slope of the refracted branch at the point of intersection of the reflected and refracted arrivals,  $h_w$  is the normal incidence water depth,  $v_w$  is the velocity in water,  $h_1$  is the normal incidence thickness of the hidden layer,  $X$  and  $T$  are the offset and twt of the point of intersection of the reflected and refracted branches, respectively, while  $x_0$  and  $t_0$  are the distance traveled and twt, respectively, for the portion of the raypath that the rays traveled in the water layer, and  $x_1$  is the distance traveled for the portion of the raypath that the wave traveled in the hidden layer (first layer).  $\emptyset$  is the dip of the seafloor in radians and is found by a least-squares fit to the equation

$$\emptyset = \sin^{-1} \left( \frac{x_r^2 - v_w^2 t(x_r)^2 + 4h_w^2}{4h_w x_r} \right), \quad (5)$$

where  $x_r$  and  $t(x_r)$  are the offset and twt vectors for points along the seafloor reflection curve.

After the hidden layer velocity structure has been calculated, the deeper or "observed" layers can be modeled. These layers are termed "observed layers" because the waves that were turned within them are seen as first arrivals on the sonobuoy records. The number of observed layers giving rise to the refraction data is difficult, if not impossible, to determine from the data. Therefore, individually stacked layers, each having a linear velocity gradient, were chosen to model the observed layers. The number of layers has been determined from a constrained quadratic spline fit to the data. The constraint on the quadratic spline fit is that the second derivative is less than or equal to zero at all points along the refracted branch. This constraint was chosen so that the crustal velocities would never be allowed to decrease with depth in the model; i.e., low velocity zones would be prevented from being present.

The number of observed layers was chosen from the number of knots used to make the constrained quadratic spline fit to the data. There were generally six knots needed to adequately fit the data, while attempting not to fit the noise in the data. The quadratic spline

function readily lends itself to calculating the linear velocity gradient of each spline piece. Six spline knots gives rise to five spline pieces, or five observed layers. The velocity gradient ( $K_n$ ), velocity at the top ( $v_{n-1}$ ), velocity at the bottom ( $v_n$ ), and thickness ( $h_n$ ) of each observed layer can be calculated from the quadratic function for each spline piece using the following formulas:

$$X = x_0 + \sum_{i=1}^{n-1} x_i + 2\sqrt{\frac{1 - p^2 v_{n-1}^2}{pK_n}} \quad (6)$$

where  $x_0$  can be calculated from equation (4) and

$$x_i = \frac{2\sqrt{1 - p^2 v_{i-1}^2} - 2\sqrt{1 - p^2 v_i^2}}{pK_i} \quad (7)$$

where  $v_i = v_{i-1} + K_i h_i$ .

Also, 
$$T(X) = t_0 + \sum_{i=1}^{n-1} t_i + \frac{2}{K_n} \ln \left| \frac{1 + \sqrt{1 - p^2 v_{n-1}^2}}{p v_n} \right| \quad (8)$$

where  $t_0$  can be calculated from equation (3) and

$$t_i = \frac{2}{K_i} \left\{ \ln \left| \frac{1 + \sqrt{1 - p^2 v_{i-1}^2}}{p v_{i-1}} \right| - \ln \left| \frac{1 + \sqrt{1 - p^2 v_i^2}}{p v_i} \right| \right\} \quad (9)$$

Equations (6) and (8) were simultaneously solved for  $K_n$ . This was performed in the tau-p domain (i.e.,  $\tau = t - px$ ) using the iterative, damped least squares technique of *Marquardt* [1963]. The smooth spline function has the added benefit of modeling a continuous velocity function throughout the layers. Since the spline is a smoothly varying function without discontinuities, then the velocity field (equal to the inverse slope of the spline function) is also without discontinuities. A plot of the digitized refracted branch and the constrained quadratic spline fit to the data is shown in Figure 6. Also shown, is the resultant velocity structure with associated uncertainties calculated from the spline fit to the data. The complete list of sonobuoy modeling results are listed in the Appendix.

## Discussion

Having interpreted over 200 sonobuoy records from the Pacific and Atlantic using the slope/intercept method, *Houtz and Ewing* [1976] have proposed that (1) the seismic structure of layer 2 consists of three sublayers 2A, 2B, and 2C having p-wave velocities of  $3.6 \pm 0.4$ ,  $5.2 \pm 0.4$ , and  $6.1 \pm 0.2$  km/s, respectively; (2) layer 2A velocities increase with age over tens of millions of years until they cannot be distinguished from velocities characteristic of layer 2B; and (3) layer 2A apparently thins with age, disappearing when velocities in layer 2A approximate those in layer 2B after about 40 m.y. [*Carlson and Jacobson*, 1994]. Their three-layer model that was based on a slope/intercept interpretation has some similarities with the model and analyses that has been demonstrated here. For example, if the upper crust consisted of three distinct layers, then the modeling using the constrained quadratic spline outlined here would have shown these three layers. In general, many more layers are need to model the upper crust, but the three layer model appears to fit the data to first order and is a good starting model.

The suggestion by *Houtz and Ewing* [1976] that layer 2A (the layer at the top of basement) becomes indistinguishable from layer 2B at approximately 40 m.y. was based for the most part, on apparent head wave arrivals from the top of basement. *Diebold and Carlson* [1993] have shown that many of these interpreted head wave arrivals may be diffraction hyperbolas or converted shear-wave arrivals, not critically refracted head waves from the top of layer 2A. So, the age-dependent variation reported by *Houtz and Ewing* [1976] may not be entirely accurate. The analyses of the sonobuoy records presented in this report can be checked for age-dependency of the velocity structure of the uppermost oceanic crust. This can be done by analyzing the age variations in the parameters determined for the hidden layer in this report. Graphs of the four hidden layer parameter (thickness, velocity at the top, velocity at the bottom, and linear velocity gradient) versus age are shown in Figure 7. Significant age variations in the hidden layer parameters do not

appear to exist from the analysis of the total sonobuoy dataset presented here. This could be explained by considering that oceanic crust formed at different portions along the EPR may be mineralogically and mechanically different, thus overprinting any systematic age dependent velocity variations. Perhaps a better check on age variations would be to analyze the velocity modeling results from a single transect running perpendicular to the ridge crest. This type of transect should sample crust that was formed at relatively the same place along the EPR. Referring back to the sonobuoy basemap (Figure 2), there is a transect that runs perpendicular to the ridge crest. This transect is located at approximately  $12^{\circ}45'N$  latitude and sampled crust ranging in age from 1 - 9 m.y. Figure 8 shows graphs of the hidden layer parameters versus age from this transect. Again, there does not appear to be any statistical age variation in the uppermost crustal velocity structure.

The  $12^{\circ}45'N$  transect velocity modeling results can also be used to check on age dependent variations in the deeper (observed) layers. If the velocity structure changes with age, then an apparent thinning or thickening of velocity isopachs with age should occur. For example, if layer 2A thins with age (as *Houtz and Ewing* [1976] stated), then the isopach from the seafloor to the 3.6 km/s (or similarly, 4.0 km/s) iso-velocity surface should thin with crustal age. Similar analyses can be done for other isopachs. A plot of the depths to the 4.0, 5.0, and 6.0 km/s iso-velocity surfaces from analyses of the northern sonobuoy transect is shown in Figure 9. The iso-velocity lines do not appear to show any statistical age variation; i.e., there is not any statistically recognizable thinning or thickening of the velocity isopachs. Thus, from the analyses of this sonobuoy dataset, there does not appear to be any statistical age variation in the velocity structure for this portion of the upper oceanic crust. This result is consistent with those stated by *Purdy* [1982] for airgun-ocean bottom hydrophone surveys at  $12^{\circ}N$  near the EPR and *Vera and Mutter* [1988] for sonobuoy and expanding spread profiles over young crust between  $11^{\circ}$  and  $13^{\circ}N$  near the EPR.

In the past, researchers have discussed age dependent mechanisms that could give rise to expected age dependent velocity variations (e.g., *Houtz and Ewing, 1976; Schreiber and Fox, 1977; Carlson and Herrick, 1990; Rohr, 1994; Grevemeyer and Weigel, 1996*). To account for the modeling results shown here, a balance of age dependent mechanisms that could give rise to the lack of p-wave velocity variations must be present. For example, infilling of voids and cracks in the layer 2A pillow basalts over time will lead to a significant density increase, thus lowering the seismic velocity; while at the same time, this added sediment and alteration products will act to stiffen the overall basalt, thus raising the seismic velocity. The overall effect could be to insignificantly change p-wave velocity. Another example stems from the effect that cracks play in determining seismic velocities. It has been shown that low aspect ratio cracks (flat cracks) lower p-wave velocities much more significantly than high aspect ratio cracks (spherical cracks) [e.g., *Walsh, 1965; Kuster and Toksoz, 1974*]. One would expect to find a higher concentration of high aspect ratio cracks in young basaltic crust (e.g., in pillows and lava tubes) than in older, more consolidated basaltic crust. This would have the effect of both reducing the total porosity with age (raising velocity) and also changing the distribution of crack aspect ratios more towards the lower end, flat cracks (lowering velocities). The net effect of reducing porosity and changing the overall crack aspect ratio distribution with age may also be to insignificantly alter the p-wave velocity of the upper oceanic crust. These are just two possible explanations for the observed lack of age dependency in the observed seismic velocities. Other mechanisms undoubtedly also affect the balance of p-wave velocity with age.

## Conclusion

Sonobuoy records taken from 20°S - 20°N along the East Pacific Rise over crust ranging in age from 0 to 10 m.y. have been digitally scanned, scaled, and modeled for upper crustal velocity structures. Modeling of the velocity structure consisted of analyses

of shipcourse navigation problems, dip moveout corrections from the seafloor reflections, and refracted or turned ray analyses. We have shown that (1) true layer 2A headwave arrivals are not present in these records, (2) the layer 2A retrograde branch reported in ESPs and other surveys cannot be resolved, and (3) layer 2B/3 velocities and average velocity gradients directly determined from the data range from 4.4 to 7.6 km/s and 1.1 to 2.2 /s, respectively. The modeling results show a lack of statistical age variations in the upper crustal p-wave velocity structure for this region along the East Pacific Rise. Several reasons could account for the lack of age variation, including density and crack aspect ratio distribution changes with age for the upper oceanic crust.

## References

- Carlson, R.L., and Herrick, C.N., 1990, Densities and porosities in the oceanic crust and their variations with depth and age: *J. Geophys. Res.*, **95**, 9153-9170.
- Carlson, R.L., and Jacobson, R.S., 1994, Comment on "Upper crustal structure as a function of plate age" by Robert Houtz and John Ewing: *J. Geophys. Res.*, **99**, 3135-3138.
- Christeson, G.L., Purdy, G.M., and Fryer, G.J., 1992, Structure of young upper crust at the East Pacific Rise near 9°30'N: *Geophys. Res. Lett.*, **19**, 1045-1048.
- Diebold, J.B., and Carlson, R.L., 1993, Layer 2A revisited: *EOS, Trans. AGU*, **74**, 603.
- Ewing, J.I., and Purdy, G.M., 1982, Upper crustal velocity structure in the ROSE area of the East Pacific Rise: *J. Geophys. Res.*, **87**, 8397-8402.
- Gravemeyer, I., and Weigel, W., 1996, Seismic velocities of the uppermost igneous crust versus age: *Geophys. J. Int.*, **124**, 631-635.
- Houtz, R., Ewing, J., and Le Pichon, X., 1968, Velocity of deep-sea sediments from sonobuoy data: *J. Geophys. Res.*, **73**, 2615-2641.
- Houtz, R., Ewing, J., and Buhl, P., 1970, Seismic data from sonobuoy stations in the northern and equatorial Pacific: *J. Geophys. Res.*, **75**, 5093-5111.
- Houtz, R., 1976, Seismic properties of layer 2A in the Pacific: *J. Geophys. Res.*, **81**, 6321-6331.
- Houtz, R., and Ewing, J., 1976, Upper crustal structure as a function of plate age: *J. Geophys. Res.*, **81**, 2490-2498.
- Jacobson, R.S., 1992, Impact of crustal evolution on changes of the seismic properties of the uppermost ocean crust: *Rev. Geophys.*, **30**, 23-42.
- Johnson, H.P., and Semyan, S.W., 1994, Age variation in the physical properties of oceanic basalts: Implications for crustal formation and evolution: *J. Geophys. Res.*, **99**, 3123-3134.
- Kappus, M.E., Harding, A.J., and Orcutt, J.A., 1995, A baseline for upper crustal velocity variations along the East Pacific Rise at 13°N: *J. Geophys. Res.*, **100**, 6143-6161.
- Kuster, G.T., and Toksoz, M.N., 1974, Velocity and attenuation of seismic waves in two-phase media: Part 1. Theoretical formulations: *Geophysics*, **39**, 587-606.
- Le Pichon, X., Ewing, J., and Houtz, R.E., 1968, Deep-sea sediment velocity determination made while reflection profiling: *J. Geophys. Res.*, **73**, 2597-2614.
- Marquardt, D.W., 1963, An algorithm for least-squares estimation of nonlinear parameters: *J. Soc. Indust. Appl. Math.*, **11**, 431-441.

- Nettleton, L.L., 1940, *Geophysical Prospecting for Oil*, McGraw-Hill Book Co., Inc., New York, 444 pp.
- Purdy, G.M., 1982, The variability in seismic structure of layer 2 near the East Pacific Rise at 12°N: *J. Geophys. Res.*, **87**, 8403-8416.
- Raitt, R. W., 1963, The crustal rocks: In Hill, M. N. (Ed.), *The Sea*, Wiley-Interscience, New York, 85-102.
- Rohr, K.M.M., Davis, E.E., and Hyndman, R.D., 1990, Structure of the upper oceanic crust on the eastern flank of the Juan de Fuca Ridge: Constraints from new multichannel seismic data (abstract): *EOS, Trans. AGU*, **43**, 1566.
- Rohr, K.M.M., 1994, Increase of seismic velocities in upper oceanic crust and hydrothermal circulation in the Juan de Fuca plate, *Geophys. Res. Lett.*, **21**, 2163-2166.
- Salisbury, M.H., and Christensen, N.I., 1978, The seismic velocity structure of a traverse through the Baby of Islands ophiolite complex, Newfoundland, an exposure of oceanic crust and upper mantle, *J. Geophys. Res.*, **83**, 805-817.
- Schreiber, E., and Fox, P.J., 1977, Density and *P*-wave velocity of rocks from the Famous region and their implication to the structure of the oceanic crust, *Geol. Soc. Amer. Bull.*, **88**, 600-608.
- Stephen, R.A., 1982, Travel-time curves for a simple sea floor model: *Marine Geophys. Res.*, **5**, 315-326.
- Talwani, M., Windisch, C.C., and Langseth, M.G., 1971, Reykjanes ridge crest: A detailed geophysical study: *J. Geophys. Res.*, **76**, 473-517.
- Vera, E.E., and Mutter, J.C., 1988, Crustal structure in the ROSE area of the East Pacific Rise: One-Dimensional travel time inversion of sonobuoys and expanded spread profiles: *J. Geophys. Res.*, **93**, 6635-6648.
- Vera, E.E., Mutter, J.C., Buhl, P., Orcutt, J.A., Harding, A.J., Kappus, M.E., Detrick, R.S., and Brocher, T.M., 1990, The structure of 0- to 0.2-m.y.-old oceanic crust at 9°N on the East Pacific Rise from expanding spread profiles: *J. Geophys. Res.*, **95**, 15,529-15,556.
- Vera, E.E., and Diebold, J.B., 1994, Seismic imaging of oceanic layer 2A between 9°30'N and 10°N on the East Pacific Rise from two-ship wide-aperture profiles: *J. Geophys. Res.*, **99**, 3031-3042.
- Walsh, J.B., 1965, The effect of cracks on the compressibility of rock: *J. Geophys. Res.*, **74**, 381-389.

# Appendix

$v_i$  is the velocity at the base of the  $i$ -th layer,

$K_i$  is the velocity gradient within the  $i$ -th layer, and

$h_i$  is the thickness of the  $i$ -th layer.

sonobuoy	age (m.y.)	water depth (km)	ave. dip (degs)	$v_0$ (km/s)	$v_1$ (km/s)	$K_1$ (/s)
28C13	0.67	2.93	-4.7	2.99	4.92	1.77
29C13	1.25	3.18	0.2	2.40	5.16	3.10
27C13	2.59	3.23	0.6	2.71	6.77	2.37
24C13	1.30	3.17	-2.3	2.56	5.65	3.10
26C13	0.92	3.04	-1.3	3.32	5.26	2.22
105V28	6.26	3.65	-0.2	2.68	4.59	2.64
11C13	0.05	3.02	-1.2	2.35	6.21	3.75
13C13	1.36	3.20	3.8	1.88	4.78	3.37
15C13	0.71	2.80	2.9	2.07	6.50	4.99
19C13	0.67	3.08	-0.3	2.79	4.61	3.24
41C13	2.81	3.44	1.0	2.27	6.60	3.41
48C13	1.36	3.01	2.7	1.81	5.36	3.68
50C13	2.01	3.07	0.1	2.51	5.76	2.36
51C20	1.24	3.13	0.1	2.90	4.41	3.51
52C20	1.33	3.29	1.7	3.24	5.73	2.56
53C20	1.59	3.41	-1.7	3.01	5.43	3.67
54C13	0.93	2.69	0.4	1.96	6.01	3.23
54C20	0.90	3.14	1.4	2.23	5.22	3.58
55C13	0.95	2.98	2.2	2.37	4.58	3.05
56C13	0.94	2.93	3.5	2.02	6.14	3.34
57V32	9.43	3.61	-0.5	1.67	6.87	2.81
58C13	1.17	2.95	5.1	1.71	4.62	2.96
59V32	10.60	3.34	3.5	1.70	5.49	2.73
60C13	1.95	3.07	-0.2	2.72	5.80	2.08
61C13	2.09	2.38	-0.7	2.15	5.20	3.13
62C13	2.24	3.14	0.9	2.40	4.84	2.94
63V32	6.72	3.47	2.3	2.12	3.92	3.29
90C13	4.50	1.04	-1.3	2.35	4.74	1.93
76C13	4.79	3.32	3.1	2.31	5.61	2.78
75C13	4.80	3.11	-1.5	3.10	5.13	1.26
75V32	8.85	3.89	0.4	2.32	5.03	1.79
70C13	4.98	3.32	3.4	2.44	5.62	2.22
72C13	5.68	3.40	-1.2	2.43	6.47	2.84
71C13	6.15	3.38	1.7	2.55	5.92	2.73
73V32	8.19	3.80	0.1	1.95	6.22	2.51
17C13	0.11	2.76	-0.3	2.23	5.84	3.60
98V28	9.92	1.89	2.0	2.09	4.41	2.32
66V32	3.16	3.80	0.0	2.39	5.21	2.50
108V28	1.96	3.22	-0.1	3.11	4.56	1.81
109V28	4.52	3.45	0.5	2.65	5.07	2.61
101V28	4.66	2.95	0.6	1.55	5.46	2.43
100V28	10.33	1.95	-0.4	1.70	4.70	3.19

<b>h1</b>	<b>v2</b>	<b>K2</b>	<b>h2</b>	<b>v3</b>	<b>K3</b>	<b>h3</b>	<b>v4</b>
<b>(km)</b>	<b>(km/s)</b>	<b>(/s)</b>	<b>(km)</b>	<b>(km/s)</b>	<b>(/s)</b>	<b>(km)</b>	<b>(km/s)</b>
1.09	4.92	0.00	0.00	4.92	0.00	0.00	4.92
0.89	5.16	0.00	0.00	5.16	0.00	0.00	5.43
1.72	6.77	0.00	0.00	6.77	0.00	0.00	6.77
0.99	5.65	0.00	0.00	5.65	0.00	0.00	5.65
0.87	5.65	1.73	0.22	5.65	0.00	0.00	6.73
0.73	4.91	3.42	0.09	5.20	0.65	0.45	5.58
1.03	6.39	0.90	0.21	6.39	0.00	0.00	6.39
0.86	4.78	0.00	0.00	4.78	0.00	0.00	4.78
0.89	6.50	0.00	0.00	6.50	0.00	0.00	6.50
0.56	4.61	0.00	0.04	5.03	2.35	0.18	5.55
1.27	6.60	0.00	0.00	6.60	0.00	0.00	6.60
0.97	5.43	0.13	0.58	5.43	0.00	0.00	5.43
1.38	5.76	0.00	0.00	5.76	0.00	0.00	6.59
0.43	4.41	0.00	0.00	4.41	0.00	0.00	4.41
0.97	5.73	0.00	0.00	5.73	0.00	0.00	5.73
0.66	5.43	0.00	0.00	5.43	0.00	0.00	5.43
1.25	6.19	0.49	0.37	6.19	0.00	0.00	6.19
0.83	5.31	2.31	0.04	7.52	0.89	2.48	7.52
0.72	5.93	0.76	1.77	6.50	0.88	0.65	6.50
1.23	6.14	0.00	0.00	6.14	0.00	0.00	6.14
1.85	6.87	0.00	0.00	6.87	0.00	0.00	7.17
0.98	4.66	2.11	0.02	4.82	0.69	0.23	5.28
1.39	5.92	1.16	0.37	6.53	1.64	0.37	6.53
1.48	8.00	0.78	2.81	8.00	0.00	0.00	8.00
0.97	5.52	0.66	0.48	5.96	0.83	0.52	6.38
0.83	5.32	0.99	0.48	6.41	1.48	0.74	7.82
0.55	4.65	1.69	0.43	4.71	1.26	0.05	4.74
1.24	4.86	0.64	0.18	4.86	0.00	0.00	4.86
1.19	5.95	1.32	0.26	6.57	1.53	0.41	7.34
1.61	5.17	2.67	0.02	5.78	0.81	0.76	5.78
1.51	5.81	1.32	0.59	5.98	1.01	0.17	6.33
1.43	5.62	0.00	0.00	5.62	0.00	0.00	5.62
1.42	6.47	0.00	0.00	6.47	0.00	0.00	6.47
1.24	6.42	1.34	0.37	6.72	1.35	0.23	7.46
1.70	6.50	0.94	0.29	6.57	0.92	0.08	6.96
1.00	5.92	1.52	0.05	6.08	0.70	0.24	6.16
1.00	4.41	0.00	0.00	4.41	0.00	0.00	4.41
1.13	5.21	0.00	0.00	6.38	1.55	0.76	6.62
0.80	4.62	1.64	0.04	5.93	1.42	0.92	6.25
0.93	5.19	0.56	0.22	5.19	0.00	0.00	5.87
1.61	5.46	0.00	0.00	5.46	0.00	0.00	5.46
0.94	4.70	0.00	0.00	4.77	0.69	0.11	5.60

K4	h4	v5	K5	h5	v6	K6	h6
(/s)	(km)	(km/s)	(/s)	(km)	(km/s)	(/s)	(km)
0.00	0.00	5.53	1.49	0.41	8.00	1.51	1.63
2.63	0.10	6.48	2.62	0.40	6.48	0.00	0.00
0.00	0.00	6.77	0.00	0.09	7.56	0.83	0.94
0.00	0.12	6.87	2.21	0.55	8.00	2.45	0.46
1.89	0.58	7.57	2.49	0.33	7.57	0.00	0.00
17.92	0.02	6.25	0.73	0.92	6.25	0.00	0.00
0.00	0.00	6.39	0.00	0.00	6.39	0.00	0.00
0.00	0.08	5.13	3.55	0.10	5.16	0.24	0.11
0.00	0.00	6.50	0.00	0.00	6.50	0.00	0.00
1.06	0.49	5.55	0.00	0.03	6.29	2.21	0.34
0.00	0.00	6.60	0.00	0.11	8.00	2.59	0.54
0.00	0.00	5.43	0.00	0.00	5.43	0.00	0.00
1.04	0.79	6.73	0.95	0.15	6.73	0.00	0.00
0.00	0.00	4.41	0.00	0.00	4.41	0.00	0.00
0.00	0.00	5.73	0.00	0.00	5.73	0.00	0.00
0.00	0.24	6.00	1.06	0.54	6.00	0.00	0.00
0.00	0.00	6.19	0.00	0.00	6.19	0.00	0.00
0.00	0.00	7.52	0.00	0.00	7.52	0.00	0.00
0.00	0.00	6.50	0.00	0.00	6.50	0.00	0.00
0.00	0.00	6.14	0.00	0.00	6.14	0.00	0.00
0.30	1.00	7.17	0.00	0.00	7.17	0.00	0.00
1.43	0.32	5.28	0.00	0.00	5.28	0.00	0.00
0.00	0.00	6.53	0.00	0.00	6.53	0.00	0.00
0.00	0.00	8.00	0.00	0.00	8.00	0.00	0.00
0.57	0.74	6.38	0.00	0.00	6.38	0.00	0.00
0.60	2.34	7.82	0.00	0.00	7.82	0.00	0.00
1.08	0.03	5.04	1.64	0.18	6.79	3.28	0.53
0.00	0.00	4.86	0.00	0.00	4.86	0.00	0.00
1.46	0.52	7.34	0.00	0.00	7.34	0.00	0.00
0.00	0.00	6.51	1.07	0.68	6.51	0.00	0.00
1.46	0.24	6.33	0.00	0.00	6.33	0.00	0.00
0.00	0.00	5.62	0.00	0.00	5.62	0.00	0.00
0.00	0.00	6.47	0.00	0.00	6.47	0.00	0.00
1.54	0.48	7.46	0.00	0.00	7.46	0.00	0.00
1.39	0.28	7.34	1.56	0.24	7.34	0.00	0.00
0.83	0.09	6.37	0.86	0.24	7.37	1.79	0.56
0.00	0.00	4.57	0.51	0.32	5.26	1.15	0.60
1.29	0.18	6.62	0.00	0.00	6.62	0.00	0.00
1.47	0.22	6.25	0.00	0.00	6.25	0.00	0.00
1.43	0.47	5.87	0.00	0.00	6.25	1.22	0.31
0.00	0.00	5.46	0.00	0.00	5.46	0.00	0.00
1.33	0.62	5.60	0.00	0.00	5.60	0.00	0.00

## Figure Captions

Fig. 1. Variable-offset airgun sonobuoy profile 105V28-B shot over 6.26 m.y. old crust at  $95^{\circ}15'W$ ,  $5^{\circ}19'N$ . The data has been bandpass filtered (5 to 20 Hz) and is composed of sign-bit (0s and 1s) traces. Note the change in gain setting at approximately 3.7 km offset, and the loss of clarity below the seafloor reflection and ringiness of the data due to air-bubble source oscillations.

Fig. 2. Locations of the variable-offset airgun sonobuoy profiles used in this research. The entire dataset lies near the East Pacific Rise over crust ranging in age from 0 to approximately 10 m.y.

Fig. 3. Plot of digitized picks at four different offsets along the observed refracted branch on the sonobuoy records. The refracted branch was picked ten times at each of the four offsets to determine the repeatability, or precision in signal picking. The uncertainty in picking was determined from the average standard deviation of the picked values. The human picking precision is slightly less than 3.0 ms.

Fig. 4. Tau-p transform of the sonobuoy record 105V28-B shown in Figure 1. This transformation was done as an attempt to better display the refracted arrivals from turned rays. This transformation of the data was unsuccessful in showing more information in the records than can be seen in the original traveltime vs. offset displays. The noise in the data appears to be even more evident in the tau-p transformation than in the original records. Thus, all analyses in this report were done on the original traveltime vs. offset records. Compare this figure with Figure 3a of *Vera and Mutter* [1988].

Fig. 5. (a) Ray path diagram and velocity model for the hidden layer approximation of *Ewing and Purdy* [1982]. It is assumed that there is a single hidden layer with a linear velocity gradient with depth present in the uppermost oceanic crust whose arrivals are masked by the seafloor reflection and are thus uninterpretable. (b) Forward model on the right of the velocity structure shown on the left. Note the triplication of the refracted branch being overshadowed by the dominant seafloor reflection. From the example in Figure 1, it is apparent that the arrivals from rays turned at shallow depths are not visible in the data.

Fig. 6. Constrained quadratic spline fit to the digitized refracted branch observed in the original sonobuoy record (SB 105V28-B) is shown in (a). This quadratic spline readily allows for the calculation of a six layer crustal velocity model - one hidden layer and five layers modeled from the spline pieces. Each layer is modeled with a linear velocity gradient. (b) Resultant velocity model with associated uncertainties represented by a velocity envelope. Any velocity function that would fall within the envelope adequately fits the data.

Fig. 7. Calculated parameters for the hidden layer as a function of crustal age for the entire dataset shown on the basemap in Figure 2. No statistical correlation was found between any of these parameters and age.

Fig. 8. Calculated parameters for the hidden layer as a function of crustal age for the northern transect at approximately  $12^{\circ}45'N$  latitude shown on the basemap in Figure 2. No statistical correlation was found between any of these parameters and age.

Fig. 9. Depth to the 4.0, 5.0, and 6.0 km/s constant velocity surfaces (iso-velocity surfaces) modeled from the northern transect dataset. From this figure, no apparent thinning or thickening of velocity isopachs with crustal age exists. Layer 2A does not appear to thin, nor does layer 2B/2C appear to thicken away from the ridge crest. Upper crustal p-wave velocity structure does not appear to be a function of crustal age for the airgun sonobuoy records analyzed in this report.

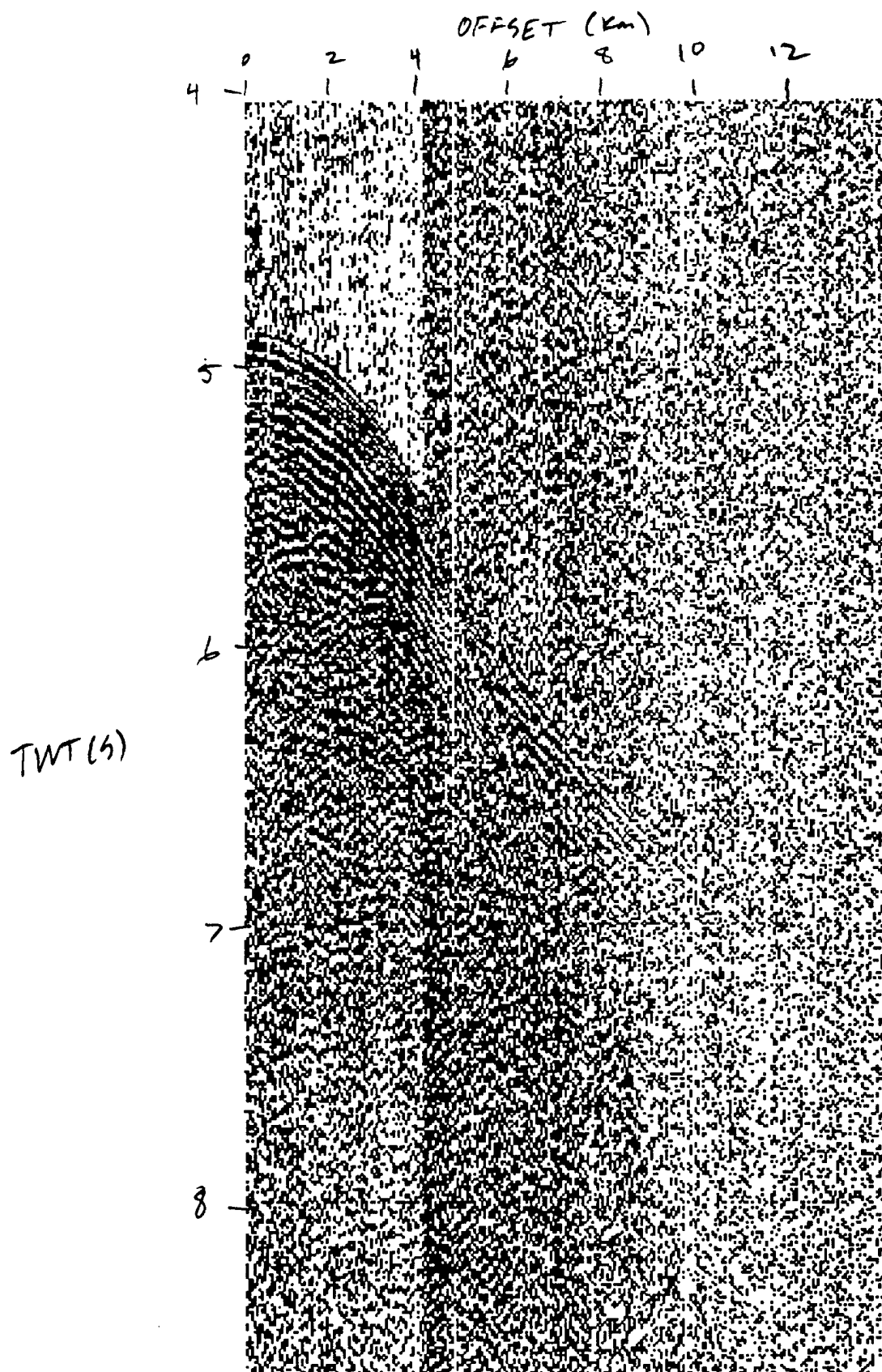


FIG. 1

# SONOBUOY BASEMAP

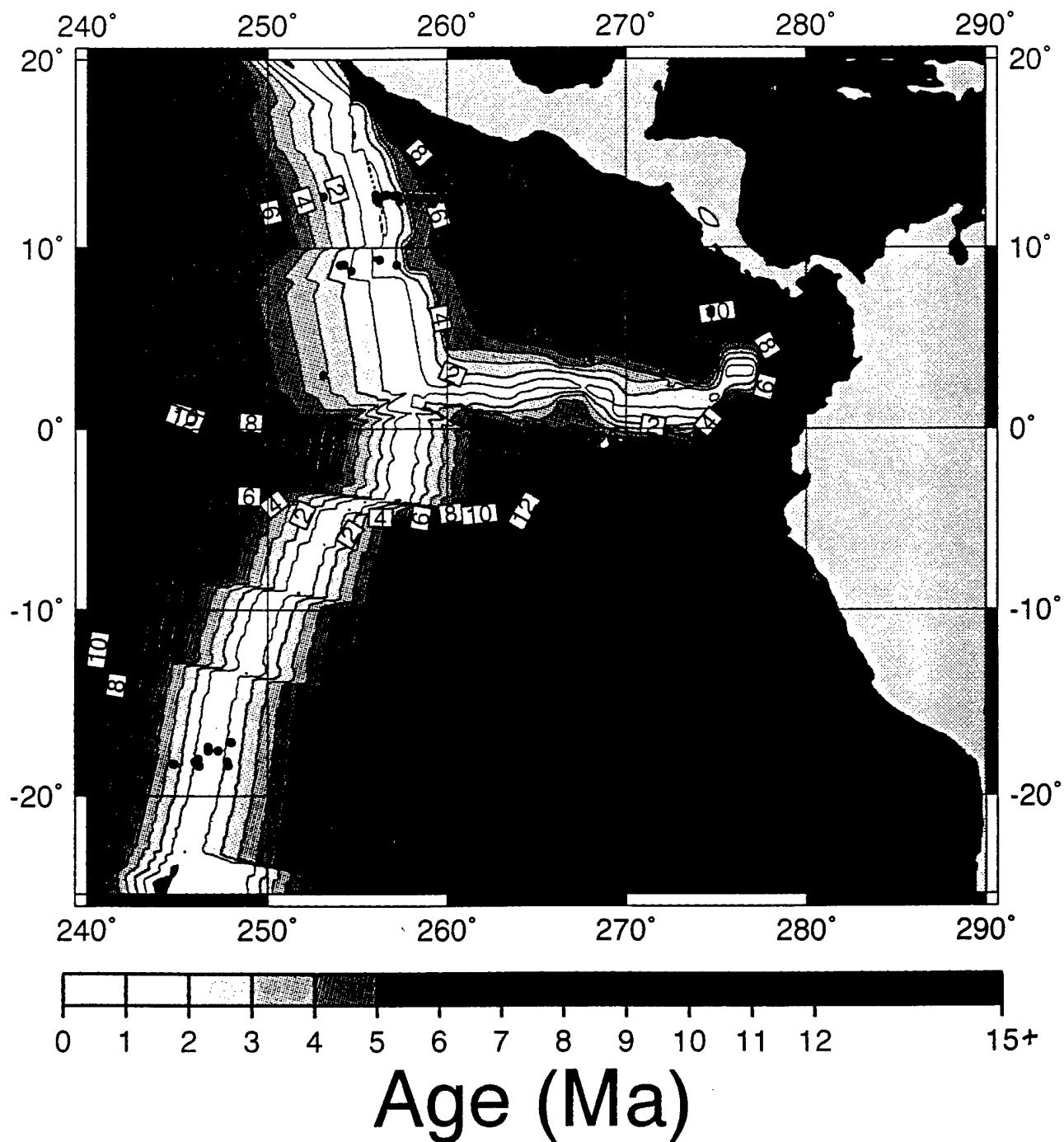
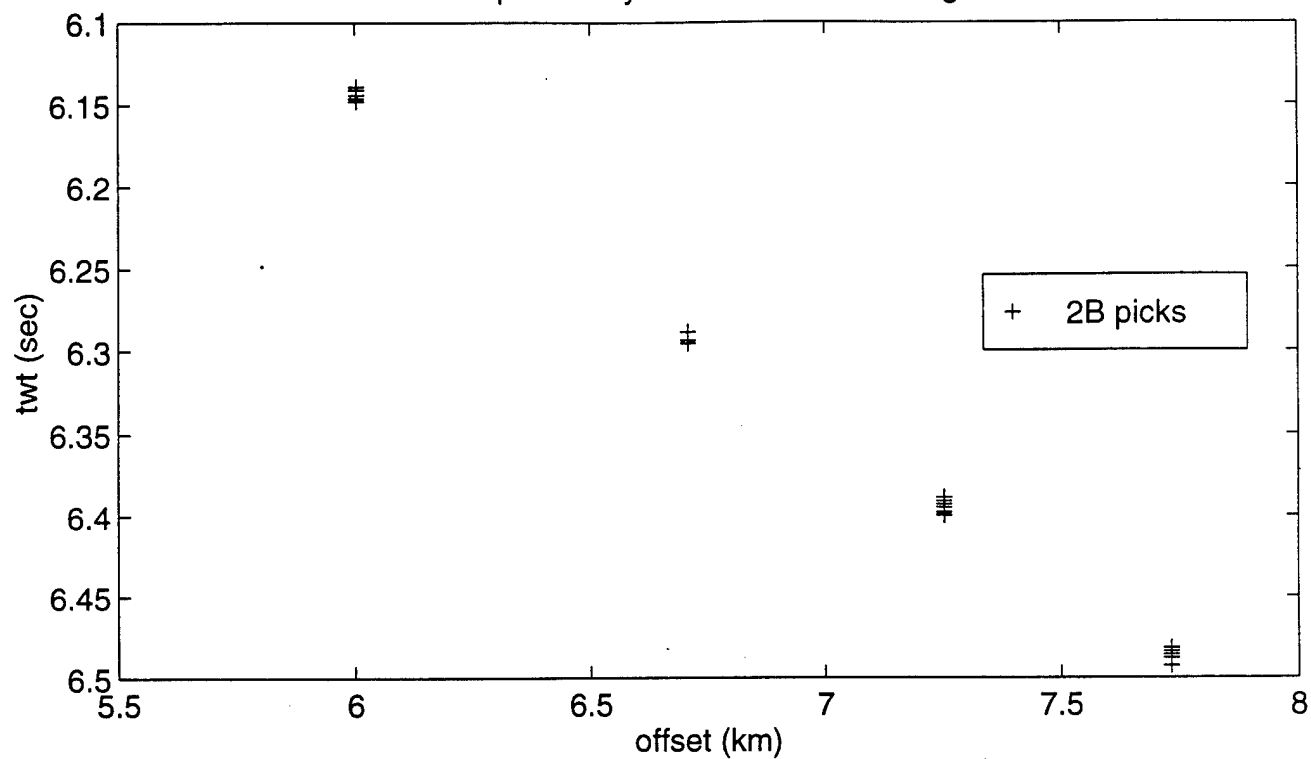
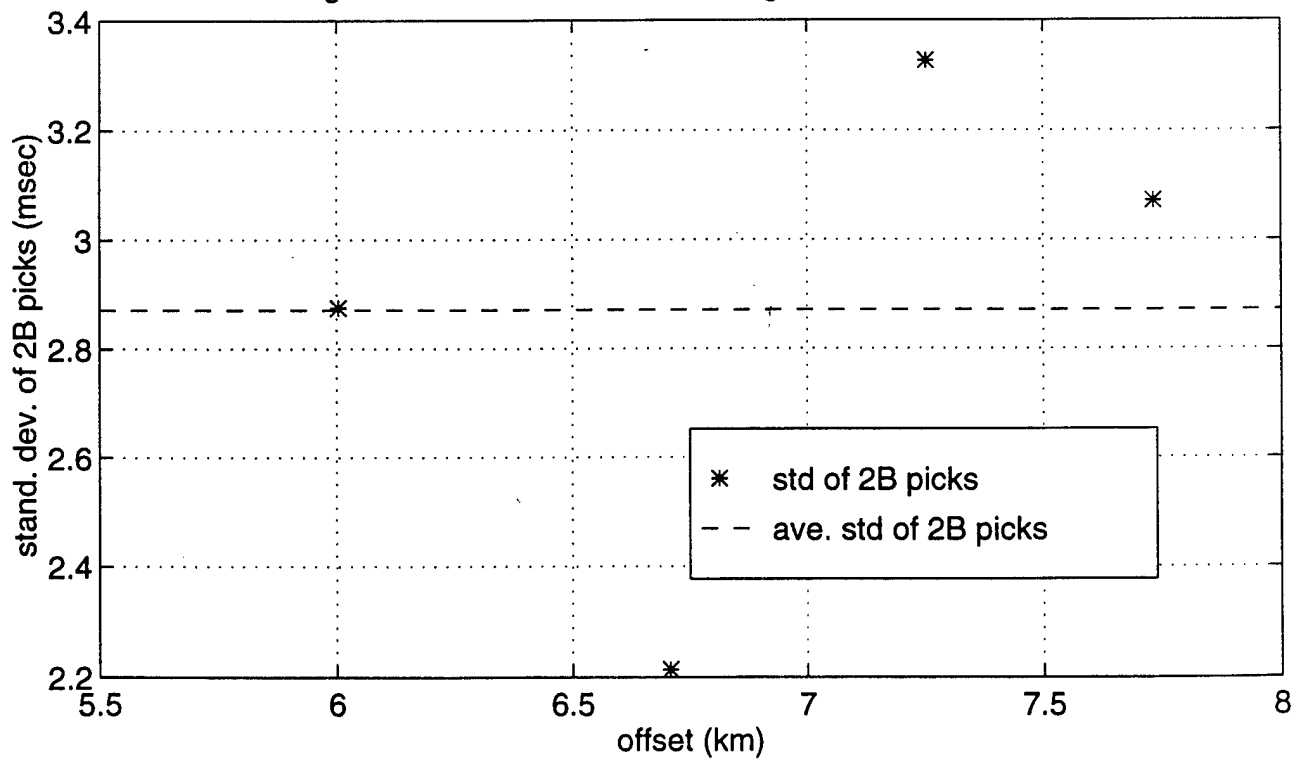


FIG. 2

Repeatability in Arrival Time Picking



Average Standard Deviation in Picking 2B Arrivals = 2.872 msec



F14.3

# Tau-p Transform for Sonobuoy 105C13-B

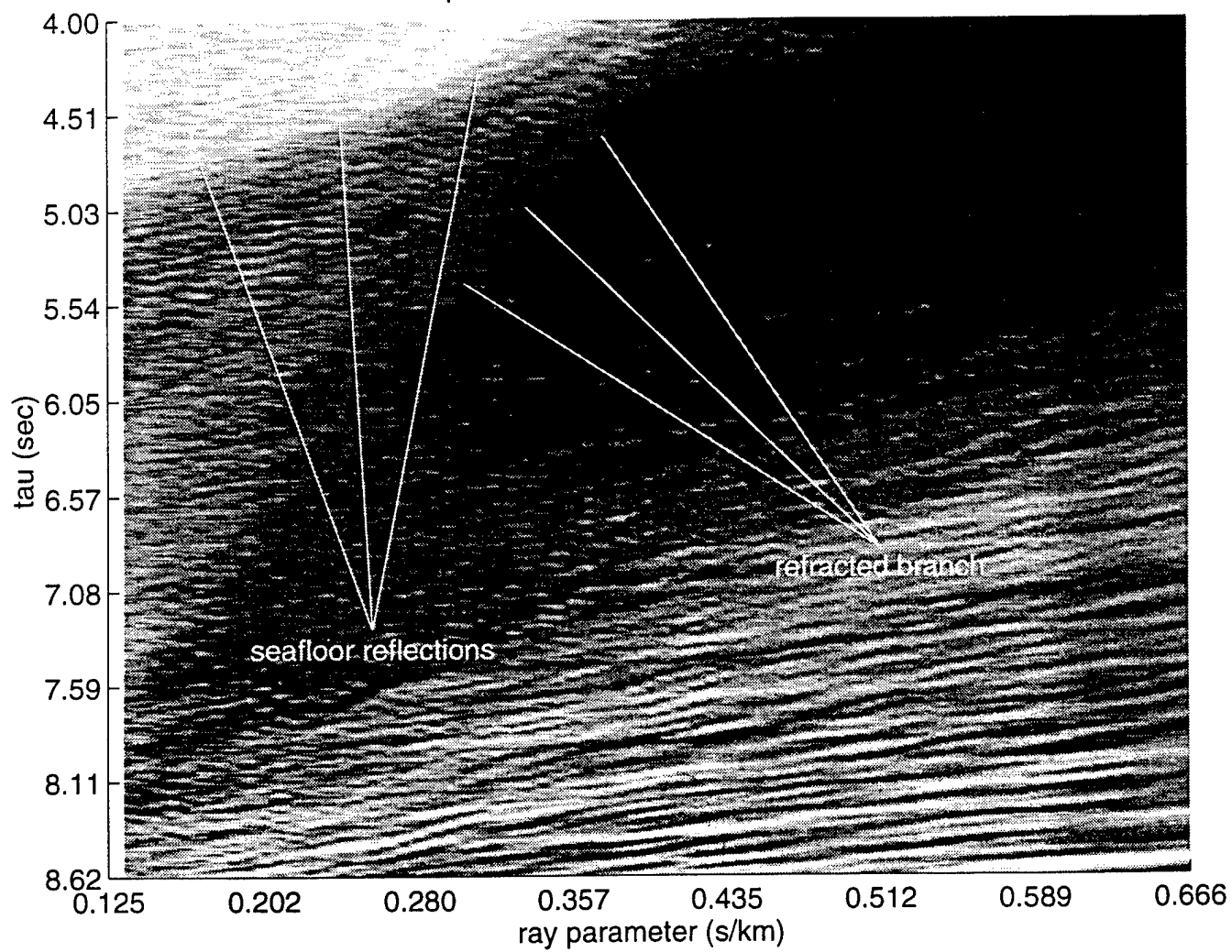
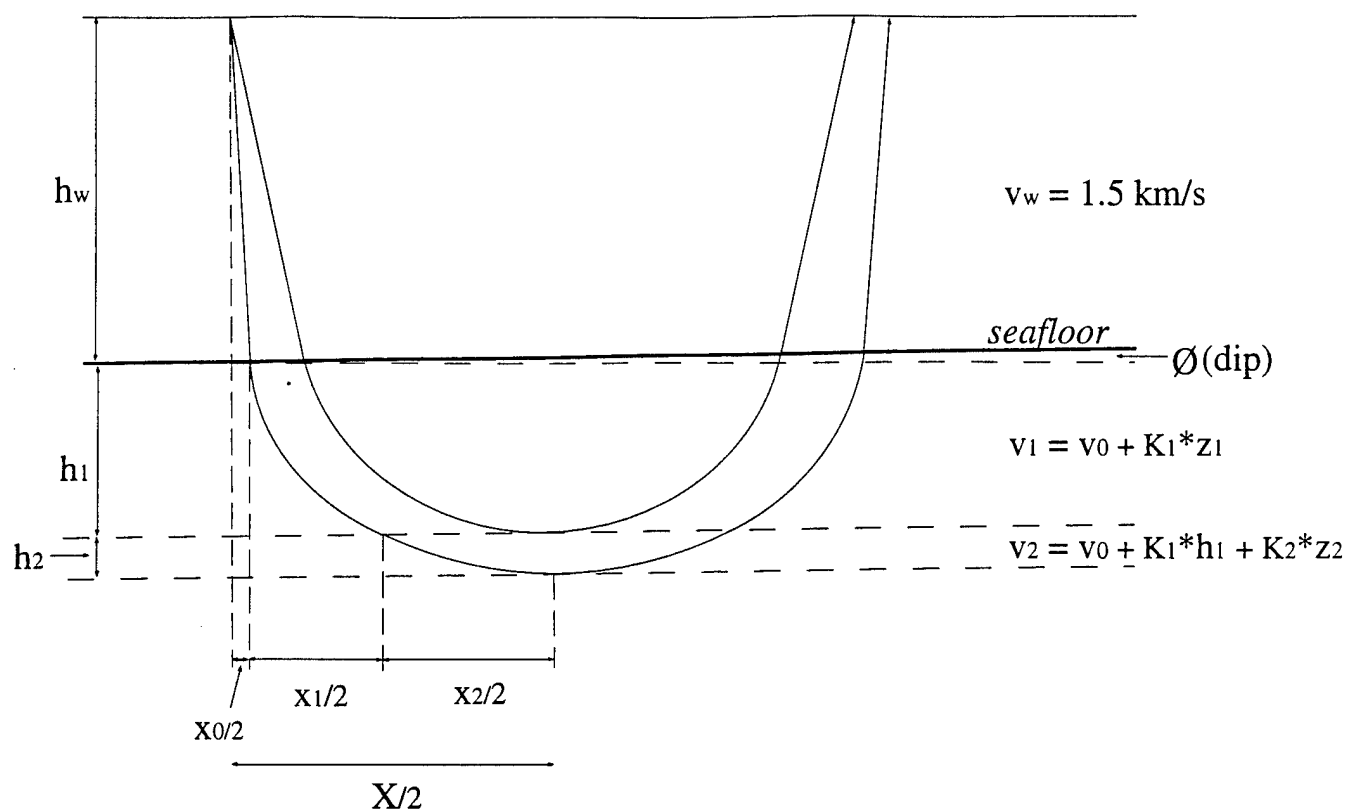
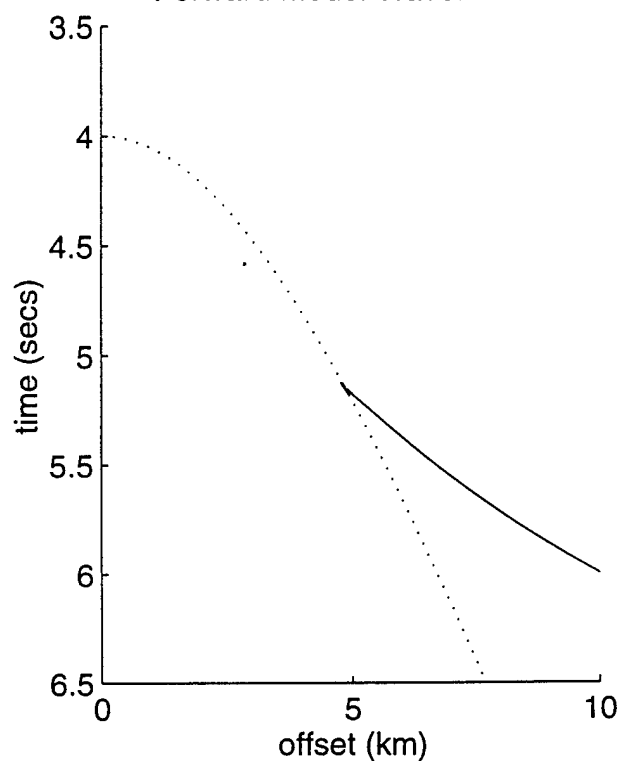


FIG. 4

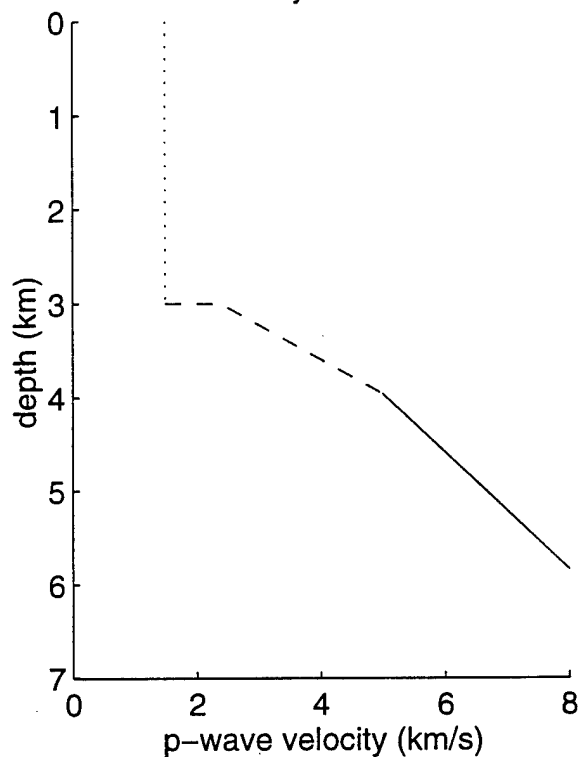


Flh. 5a

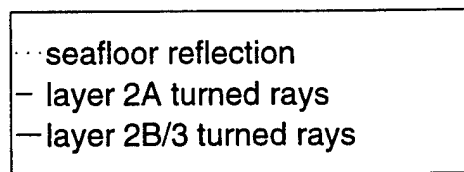
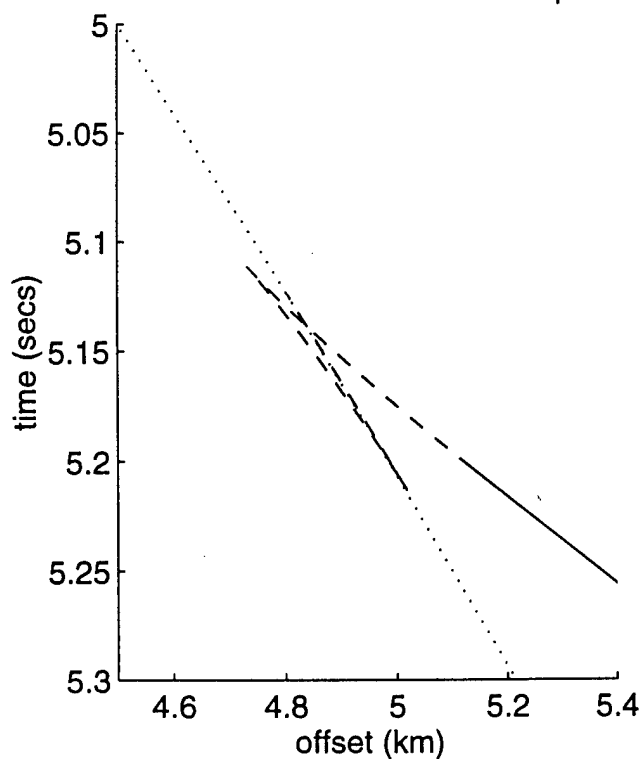
Forward Model Travel Times



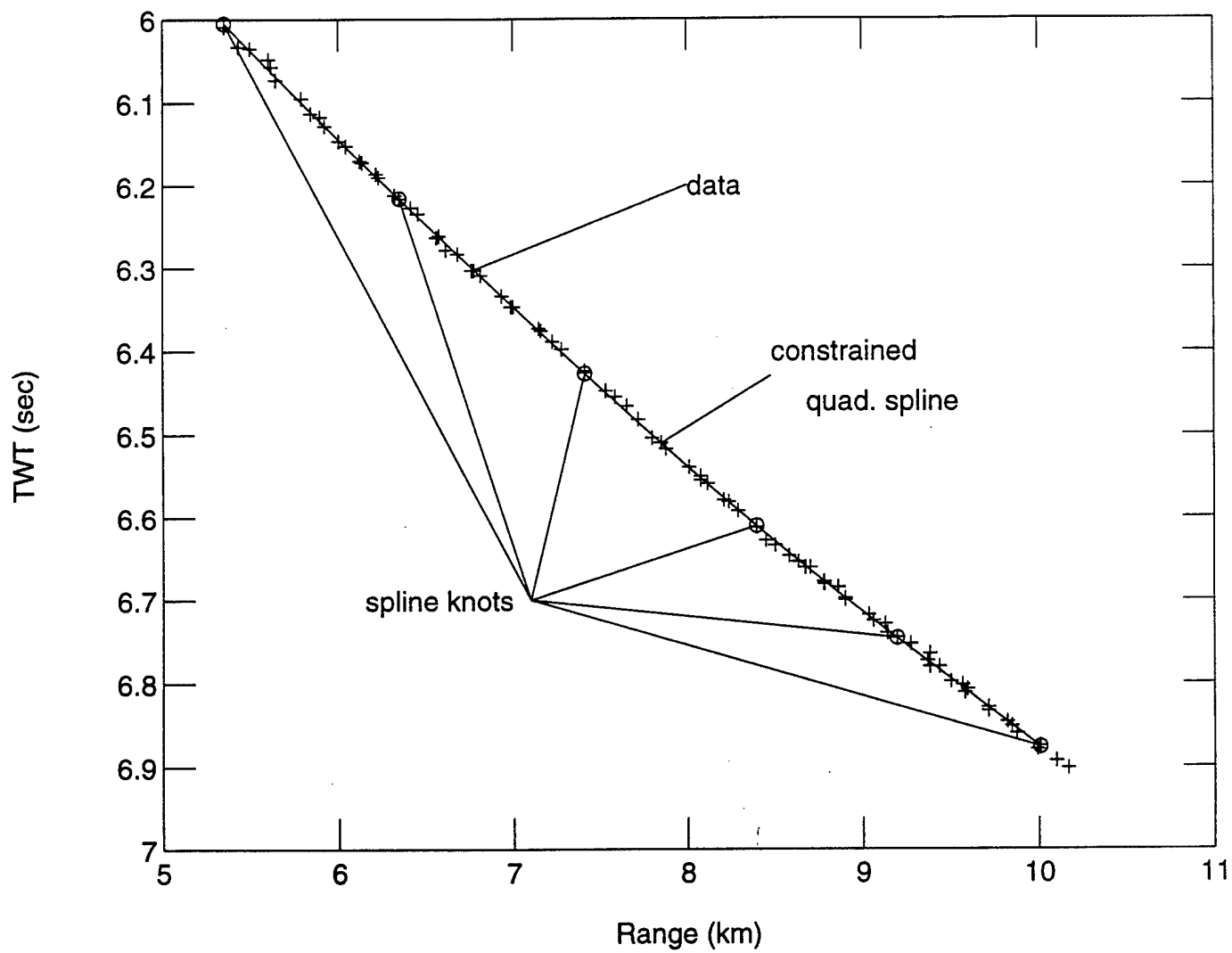
Velocity Structure



Forward Model Travel Times – Triplication



SB 105V28-B; RMSError = 3.793 msec



F/6.6a

Velocity Structure from SB 105V28-B

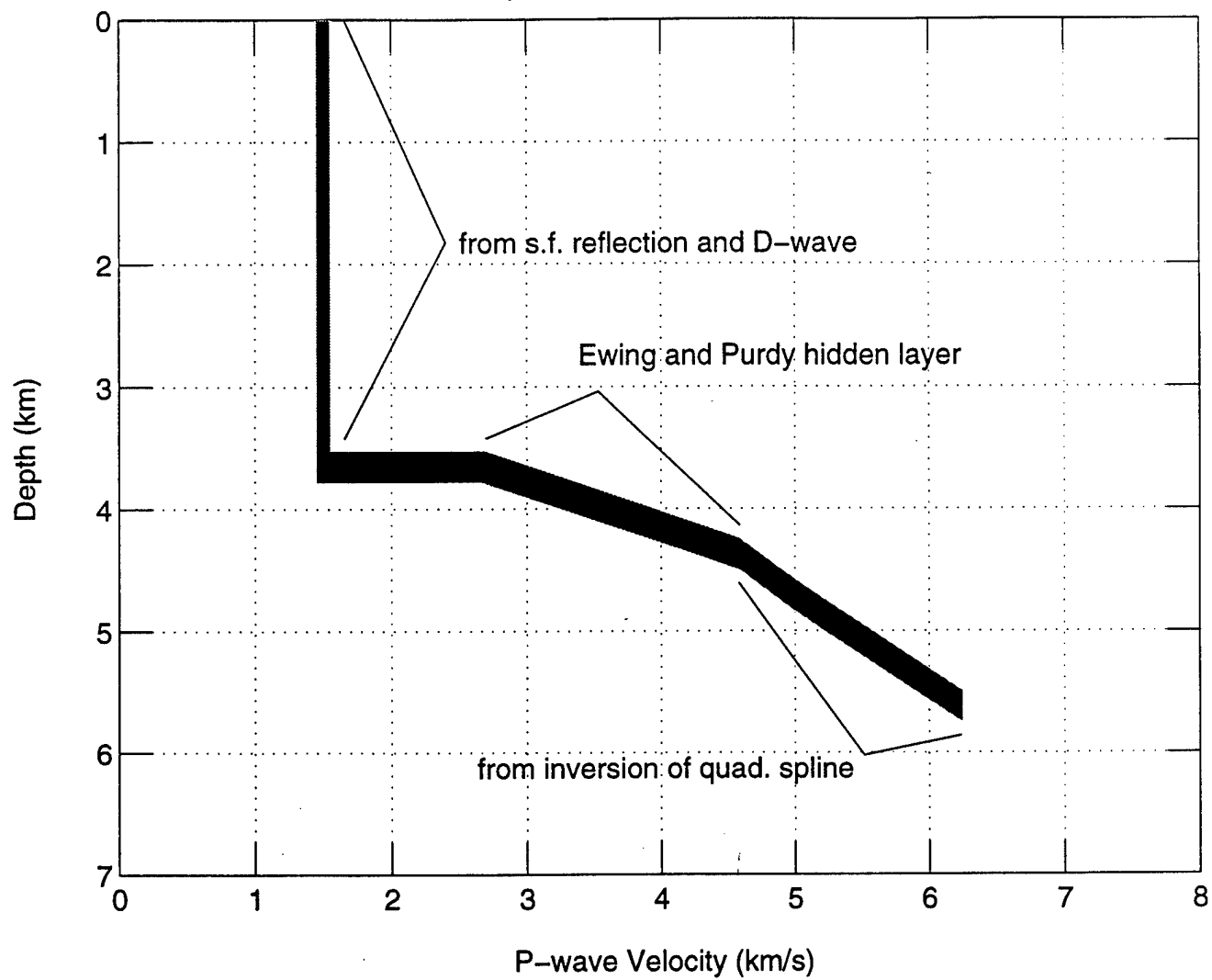
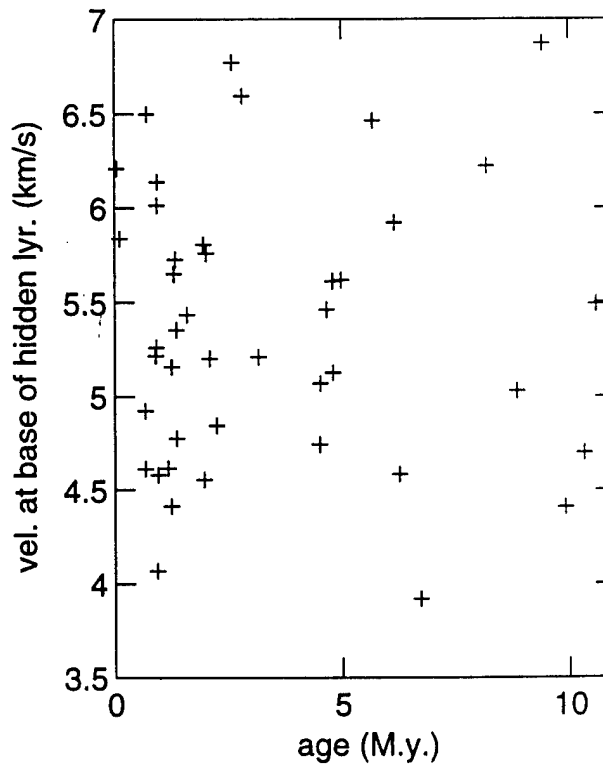
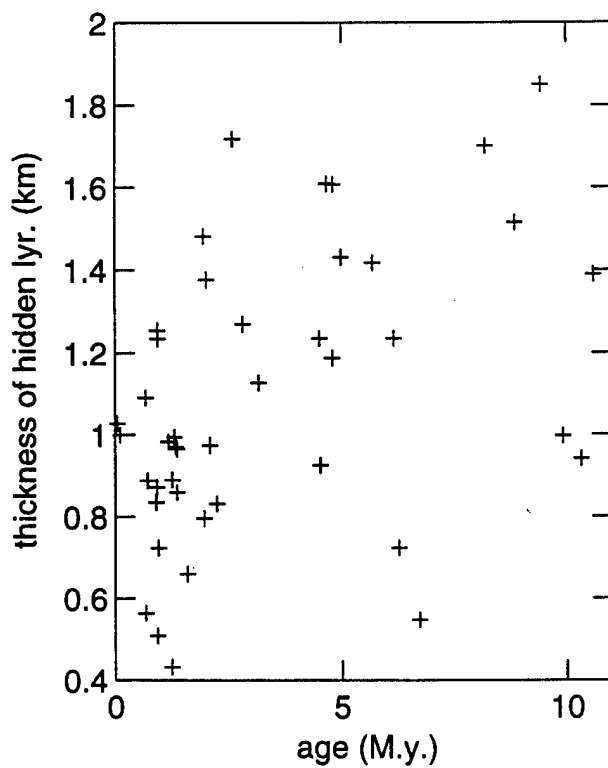
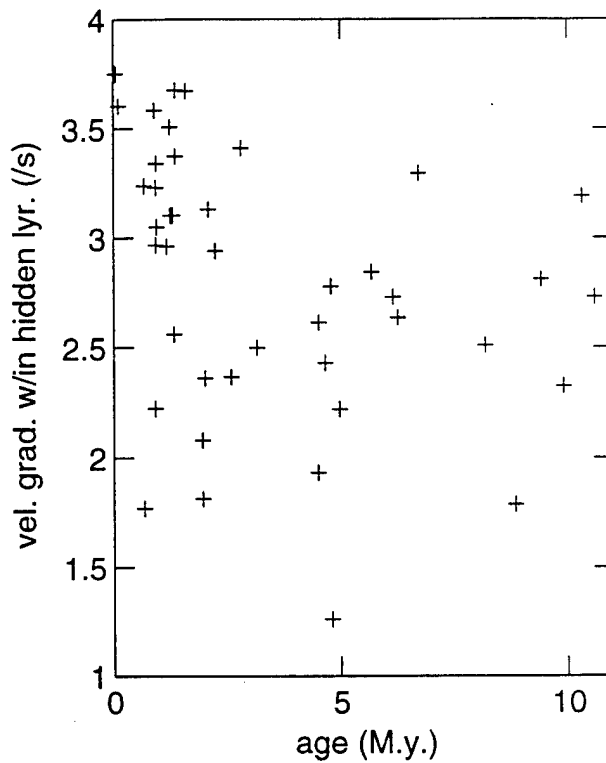
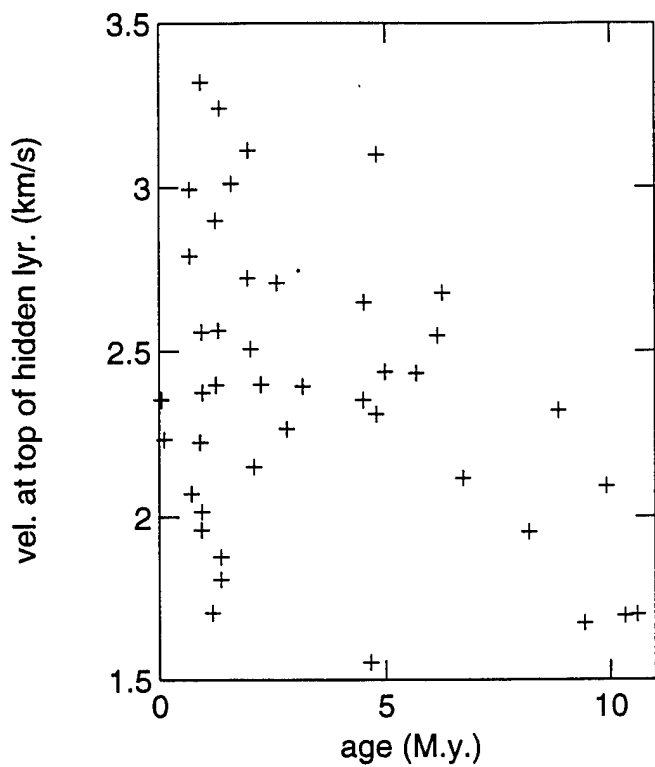
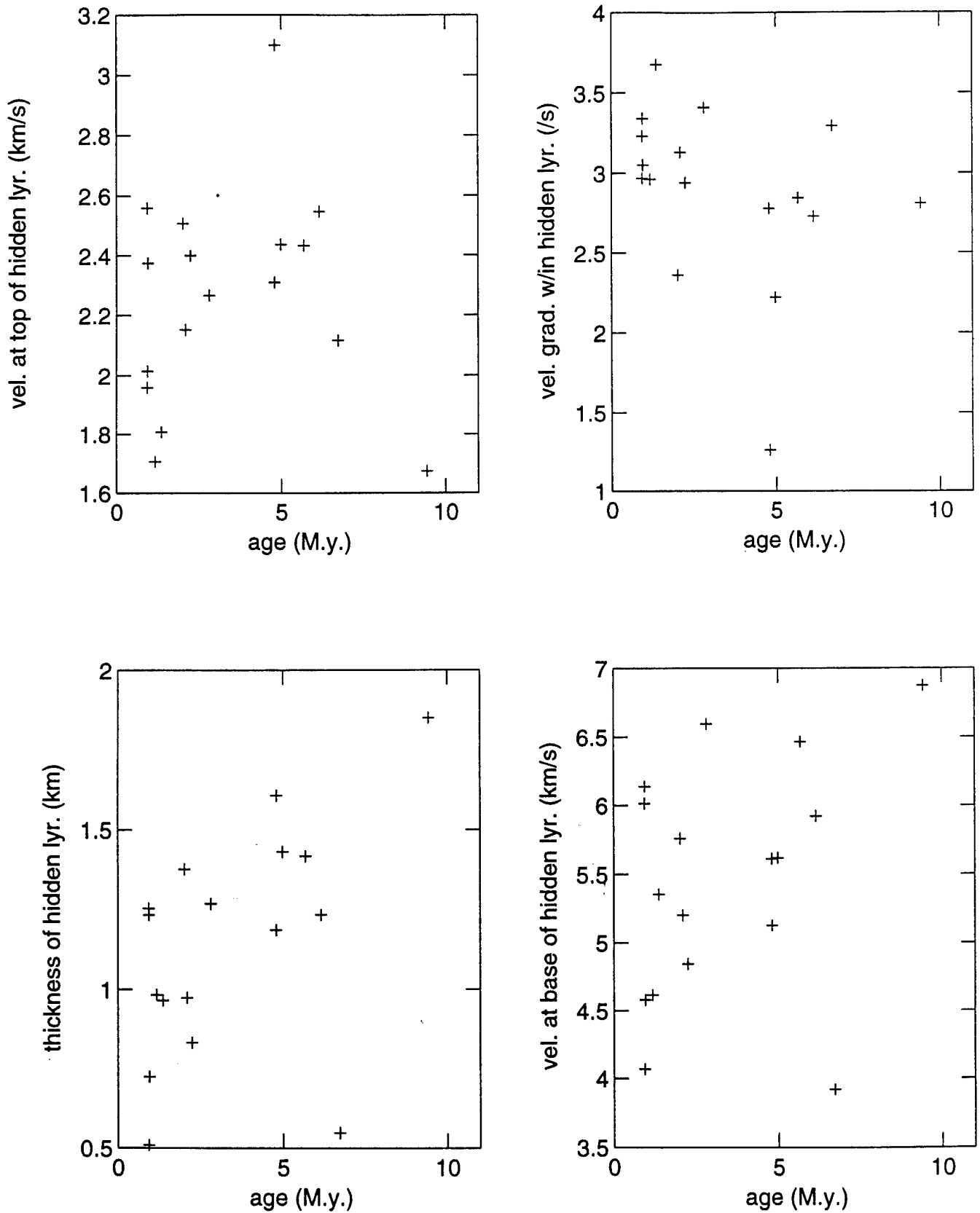


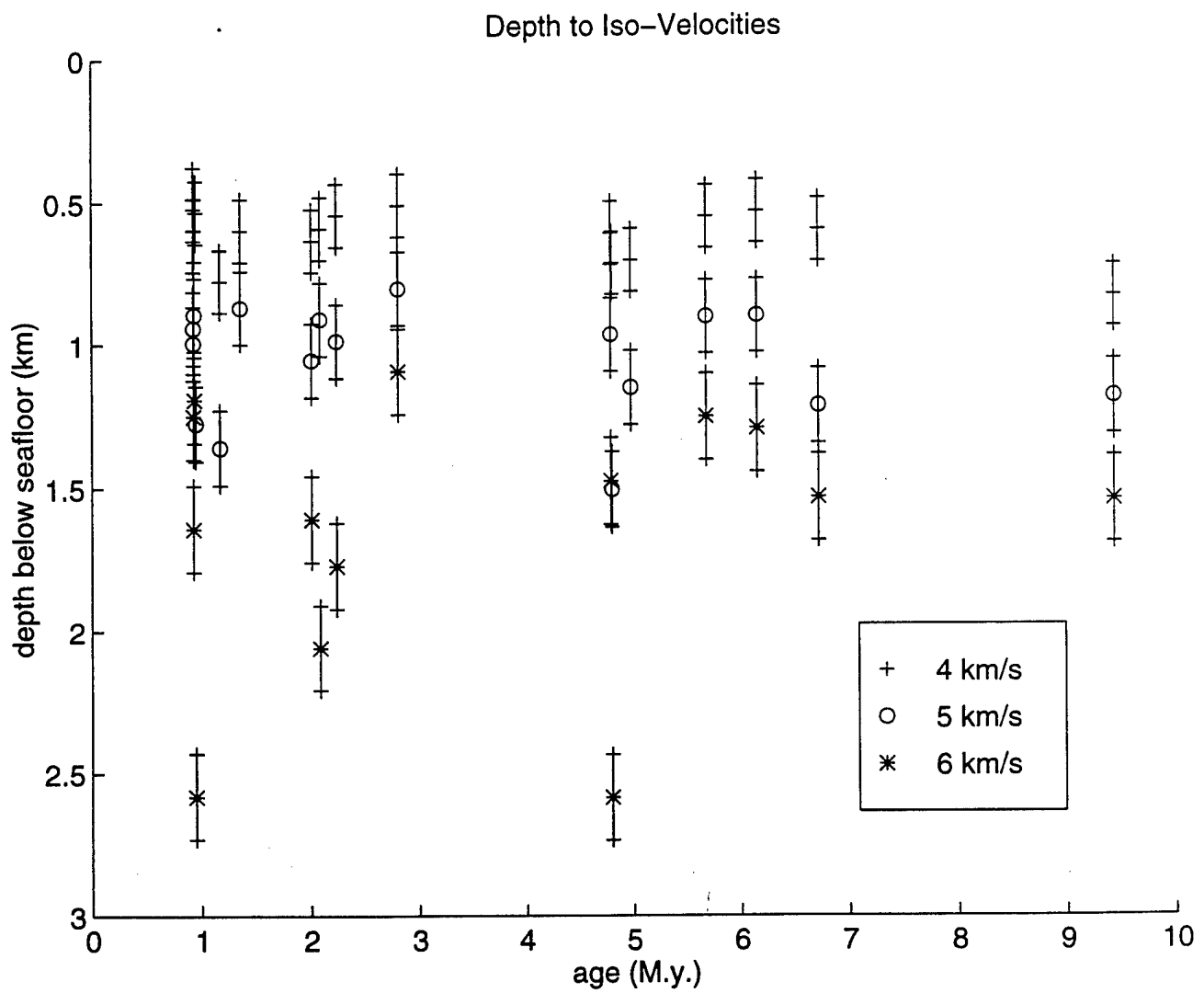
Fig. 6b

# Parameters vs. Age



# Parameters vs. Age





F16.9